Article:
Hu, H., Weng, J. and Zhang, J. (2016) Coverage Performance Analysis of FeICIC Low Power Subframes. IEEE Transactions on Wireless Communications, 15 (8). pp. 5603-5614. ISSN 1536-1276

https://doi.org/10.1109/TWC.2016.2562619

Coverage Performance Analysis of FeICIC Low Power Subframes

Haonan Hu[1,2], Jialai Weng[2], Jie Zhang[2]
[1]School of Communication and Information Engineering, Chongqing University of Posts and Telecommunications, Chongqing, China
[2]Dept. of Electronic and Electrical Engineering, The University of Sheffield, Sheffield, UK
Email:{haonan.hu,jialai.weng,jie.zhang}@sheffield.ac.uk

***Abstract*—Although the Almost Blank Subframes (ABSF) proposed in heterogeneous cellular networks can enhance the performance of the Cell Range Expansion (CRE) User Equipments (UEs), it significantly degrades macro-cell total throughput. To address this problem, the Low Power Subframes (LPSF) are encouraged to be applied in macro-cell center region by the Further-enhanced Inter-cell Interference Coordination (FeICIC). However, the residual power of the LPSF which interferes the CRE UEs, and the proportion of the LPSF affect the downlink throughput together. To achieve a better rate coverage probability, appropriate LPSF power and proportion are required. In this paper, the analytical results of the overall Signal to Interference and Noise Ratio (SINR) coverage probability and the rate coverage probability are derived under the stochastic geometric framework. The optimal region bias ranges for maximizing the rate coverage probability are also analysed. The results show that the ABSF still outperform the LPSF in terms of rate with the optimal range expansion bias, but lead to a heavier burden on the back-haul of the pico-cell. However, with a static range expansion bias, the LPSF provide better rate coverage than the ABSF. Also, in a low range expansion scenario, the reduced power of the LPSF has negligible effect on the rate coverage with the optimal resource partitioning.**

***Index Terms*—FeICIC, low power subframes, stochastic geometry, Poisson point process, Signal-to-Interference-plus-Noise Ratio.**

I. Introduction

With the proliferation of smart devices, downlink data traffic demand, for instance, video or game applications, becomes a growing concern in future cellular networks. Heterogeneous networks (HetNets), composed of traditional macro base stations (BSs) and several different low transmitting power BSs are envisioned to be a powerful tool to meet the network traffic demand. The lower power BS leads to a smaller coverage area, but provides a better data throughput because of the closer serving distance [1]. However, the smaller coverage area, especially for open access mode pico-cells, results in fewer associated UEs. It is undesirable when macro-cells are already overloaded. In order to deal with this load imbalance, the CRE is adopted. It employs a cell range bias which extends coverage area of the pico-cell without increasing transmitter power [2]. Unfortunately, in this CRE region, the UEs become more vulnerable to interference from the underlaid macro BSs. To mitigate such interference, 3GPP Release 10 states that the ABSF, with no power transmitting on data channel at some coordinated time slots, should be leveraged in macro-cells. However, the degraded performance of macro-cells caused by the ABSF, is brought into consideration in the literature recently. In 3GPP Release 11, the FeICIC is proposed. It advocates the allocation of the LPSF, instead of the ABSF, to macro-cell center region UEs at the coordinated time slots. It has been shown that the LPSF improves the the macro-cell total throughput [3].

A. Motivation and Related Works

Employing relatively high power LPSF will result in significant interference on the CRE UEs in spite of the macro-cell total throughput enhancement, which translates into lower SINR. In some worst cases, even basic modulations will be exacerbated. Furthermore, the desirable SINR does not necessary mean a qualified downlink throughput, which is also determined by the average allocated subframes directly. Therefore, analysing the overall SINR and rate coverage becomes critical.

Various approaches have been studied to analyse cellular network performance. Traditionally, the positions of BSs are modelled as hexagonal grid model [4]. Under such a deterministic grid model, Monte Carlo simulations run numerous times to obtain the statistical results, which is both time-consuming and resource-consuming. Moreover, the actual network deployment varies significantly from different cities, and the grid model can only give an optimistic performance analysis. Recently, stochastic geometry is proved to be effective for network deployment, especially the Poisson point process (PPP), capable of modelling the pessimistic network performance [5]. Using the PPP, the performance analysis of the CRE and the ABSF has been investigated in the literature. The work [6] first developed a framework for multi-tier cellular network downlink SINR analysis with the CRE. Based on this, the rate distribution of the downlink HetNets with CRE is analysed in [7]. The optimal bias value for offloading is also given but without considering ABSF. Motivated by this, the offloading problem is analysed in [8] considering both the ABSF and the CRE. However, all the aforementioned works assume a full buffer model in the BS. The work [9] analysed the offloading performance in a lightly-loaded network based on satisfying the minimum rate requirement. In [10], the load balancing is formulated as a traditional optimisation problem and the primal-dual distributed algorithms are proposed, which run on both the users and BSs.

However, only few works [4], [11], [12] analyse the performance of systems using the LPSF. Through hexagonal grid model simulation results from [4], [11], it is proved that the 5th percentile and the median throughput improve. On the other hand, there is only one work [12] using stochastic geometry to study the total capacity and the 5th percentile throughput of the FeICIC. Similar to [13], it allocates partitioning resources based on the presetting SINR value level. As a result, it is impractical to analyse the coverage performance based on the framework proposed in [12].

Despite the aforementioned research works, the study of the overall SINR and rate coverage probability of the FeICIC is missing in the literature, especially when the LPSF are employed. By employing the stochastic geometry, this work provides system design insights for the FeICIC scheme.

B. Contributions

In this work, we investigate the performance of the FeICIC when the LPSF are employed, under the stochastic geometry framework. Initially, we propose a new user association method in the FeICIC by both the power reduction and the macro-cell center region factors. It extends the dominant interferer definition in [14]. We derive an analytical expression of the overall SINR and rate coverage probability in an integral form of the threshold, the power reduction factor, the path-loss exponents, the range expansion factor and the center region factor. An approximation of the Gauss hypergeometric function is applied to obtain numerical integration results. Based on the result, optimal values of the center region bias and the range expansion bias are obtained for maximizing the rate coverage probability. Furthermore, we propose an efficient single-iteration optimisation method to obtain these near optimal values. To our best knowledge, we are the first to discuss the optimal biases under the distance-based user association strategy. Eventually, we analyse the rate coverage performance with optimal biases and static range expansion bias respectively with comparison to the ABSF.

C. Organization

The rest of paper is organized as follows: Section II introduces the system model and the user association strategy. Section III presents the derivation of the analytical results and the optimal bias ranges. Section IV gives the simulation results before concluding in Section V.

II. System Model

We consider a two-tier heterogeneous system consisting of macro-cells and pico-cells, modelled as two identically independent distribution (i.i.d) PPPs, denoted by $\mathcal{M}$ and $\mathcal{P}$ with density λ_m and λ_p respectively. They commonly share all the frequency resources. The full transmitter power of macro BSs and pico BSs are denoted by P_m and P_p, respectively. The macro-cells adopt the LPSF in center areas, with the power reduction factor ρ. Otherwise, the macro and pico BSs transmit at the fixed maximum power. With the assumption of Rayleigh fading, the received power of an arbitrary UE

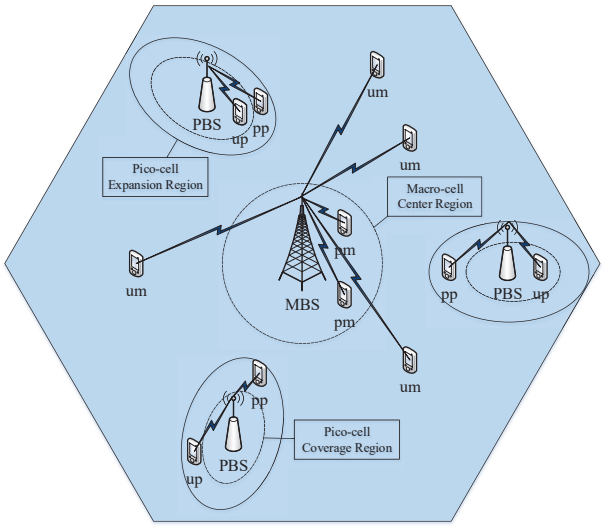

Fig. 1. User association strategy

from a BS can be represented as $Phr^{-\alpha}$. The variable h denotes the fast transmitting attenuation on received signal power following $h \sim \exp(\mu)$. The term $r^{-\alpha}$ is the large scale path-loss, where r is the Euclidean distance and α is the path-loss exponent. Shadowing is ignored to avoid loss of tractability [6]. Moreover, every cell is assumed to employ a strict synchronization scheme [8] to coordinate interference between different resources. Under such an assumption, subframes with and without power reduction cause no interference to each other. In other words, the transmitting power of protected subframes will not interfere the user using unprotected subframes, and vice versa. If the LPSF among all macro BSs are not completely aligned, the center macro UEs and the edge pico UEs (both use the LPSF) will suffer severe interference from the neighbouring macro BSs. In particular when the pico BSs are deployed at the edge region, its users still suffer full power interference from the neighbouring macro BSs. Therefore, the misaligned model is not appropriate for the pico-cell deployment scenario. On the other hand, even if the LPSF are not fully aligned, we can still reach the results as in [12] by modelling with a fraction of the full power interference. However, it is obvious that the fully aligned model performs better than the misaligned model. The full power aggregate interference from other MBSs and PBSs are denoted as I_m and I_p, respectively, and σ^2 represents the thermal noise. Then the common SINR expression can be represented as:

$$\Phi_l = \frac{\rho_l P_l h r_l^{-\alpha_l}}{\rho_l' I_{m_l} + I_{p_l} + \sigma^2}. \tag{1}$$

Similar to [12], in macro-cells, subframes with and without power reduction are defined as protected and unprotected subframes (PSF and USF), respectively. The PSF and the USF are also defined in pico-cells although such subframes with different power do not exist. It is based on the time slots as the PSF and the USF transmitted in macro-cells. In other words, the subframes transmitted in pico-cells at the same time slots

as the LPSF in macro-cells are defined as the PSF, and the other subframes are defined as the USF. In such a case, the UEs are classified into four groups: protected subframe macro-cell UEs, unprotected subframe macro-cell UEs, protected subframe Pico-cell UEs and unprotected subframe pico-cell UEs. We use the index $l \in L = \{pm, um, pp, up\}$ to denote the four corresponding UE groups. Fig. 1 illustrates the four UE groups and their relationships to the macro-cell and the pico-cell. As shown in Fig. 1, closer center region associated UEs adopt the PSF in macro-cells to mitigate interference from other BSs. In contrast, PSF in pico-cells are allocated to the CRE UEs, who receive less signal power from the serving BS. The other UEs will be allocated with the USF, i.e., the pico-cell coverage region.

Then the SINR expressions for the four UE groups can be written as:

$$\Phi_{pm}=\frac{\rho P_m h r_m^{-\alpha_m}}{\rho I_{m\backslash\{0\}} + I_p + \sigma^2}, \qquad \Phi_{um}=\frac{P_m h r_m^{-\alpha_m}}{I_{m\backslash\{0\}} + I_p + \sigma^2},$$
$$\Phi_{pp}=\frac{P_p h r_p^{-\alpha_p}}{\rho I_m + I_{p\backslash\{0\}} + \sigma^2}, \qquad \Phi_{up}=\frac{P_p h r_p^{-\alpha_p}}{I_m + I_{p\backslash\{0\}} + \sigma^2}, \tag{2}$$

where $I_{s\backslash\{0\}}$ denotes the aggregate interference excluding the serving BS. Since there is no cross-interference between the PSF and the USF, the value of ρ_l is determined as $\rho_l = \rho$ only if $l = pm$, and $\rho_l{}' = \rho$ if UE utilizes PSFs. Otherwise, $\rho_l = \rho_l{}' = 1$.

We assume that the same group users share the same spectrum resources in a round-robin manner [8]. Thus statistically the subframes can be considered to be allocated equally to the same group users, as the same group users have equal probability to obtain each subframe. By information exchange between the BSs and the UEs, the BSs know which UEs are allocated with USF and which UEs are allocated with PSF. Also we assume that the BSs know which subframes are configured as PSF and USF. Thus the scheduler runs round robin scheduling for PSF and USF users separately. Also, the BSs are assumed to follow a full buffer model, which always have backlogged data to transmit. In order to define the downlink throughput together with these SINR expressions, the resource partitioning factor (the proportion of the LPSF) is denoted as β. The probabilities of time-domain subframes configured as the PSF and the USF are β and $(1-\beta)$, respectively. Then the common throughput expression can be formulated as:

$$R_l = \frac{\beta_l W}{N_l} \log_2(1 + \Phi_l), \tag{3}$$

where β_l equals β and $1-\beta$ when using the PSF and the USF respectively. W is the spectrum bandwidth and N_l represents the number of serving UEs, which will be discussed in Section III.

A. User Association Strategy

In this subsection we introduce a user association strategy, which defines the principle of the classification of a specific UE.

Throughout our analysis, we assume that a UE is placed at the origin position. It is a reasonable assumption because there is no difference in property observed either at a point of the PPP or at an arbitrary point, according to Slivnyak's theorem [15]. Thus the UE association strategy is dependent on its nearest distances to the macro BSs and the pico BSs, denoted by r_m and r_p respectively. Thereby the user association strategy is proposed for the two-tier network scenario. For the four user groups, we define the following association strategy based on the distances and range factors as:

Proposition 1. *The UE's associated BS and allocated subframes follow the relationships between r_m and r_p as* (4) *below, where k_c, k_e and k_p are the macro-cell center region factor, the pico-cell range expansion region factor and the pico-cell coverage region factor, respectively.*

$$l = \begin{cases} pm, \text{ when } k_c r_m < r_p \\ um, \text{ when } k_e r_m < r_p < k_c r_m \\ pp, \text{ when } k_p r_m < r_p < k_e r_m \\ up, \text{ when } k_p r_m > r_p \end{cases} \tag{4}$$

The size of the macro-cell center region is completely dependent on k_c. A larger k_c results in a smaller size of the macro-cell center region. Therefore, the PSF MUEs can be limited close to their associated macro BSs by a large enough k_c, even if their nearest interfering pico BSs are distant. The value of k_e influences both the sizes of the pico-cell coverage region and the macro-cell coverage region. The value of k_p determines the coverage bound between the pico-cell coverage region and the range expansion region. In the pico-cell coverage region, the USF PUEs receive higher power from their associated pico BSs than any other macro BSs. Therefore, when a UE is deployed on this coverage region bound, its received power from the nearest macro BS $P_m(k_p r_b)^{-\alpha_m}$ equals the power from the associated pico BS $P_p {r_b}^{-\alpha_p}$, where r_b is the distance between the UE at the bound and its associated pico BS. If $\alpha_m = \alpha_p = \alpha$, the value of k_p is represented as $(P_p/P_m)^{1/\alpha}$. Otherwise, k_p has an approximation value of $(P_p/P_m)^{2/(\alpha_m+\alpha_p)}$ [14].

In order to obtain the probability for each association case, the following lemma is proposed.

Lemma 1. *In two i.i.d. PPPs Θ_i and Θ_j with density λ_i and λ_j, respectively, if the closest distances from an arbitrary point to the PPPs are denoted as r_i and r_j, then the probability of $r_i > k r_j$ is given as:*

$$\textit{Prob}(r_i > k r_j) = \frac{\lambda_j}{\lambda_j + k^2 \lambda_i}. \tag{5}$$

Proof. See Appendix A. □

The association probability for the USF MUEs and the PSF PUEs can be calculated by $\text{Prob}(k_a r_m < r_p < k_b r_m) = \text{Prob}(r_p > k_a r_m) - \text{Prob}(r_p > k_b r_m)$. Combining (5) with

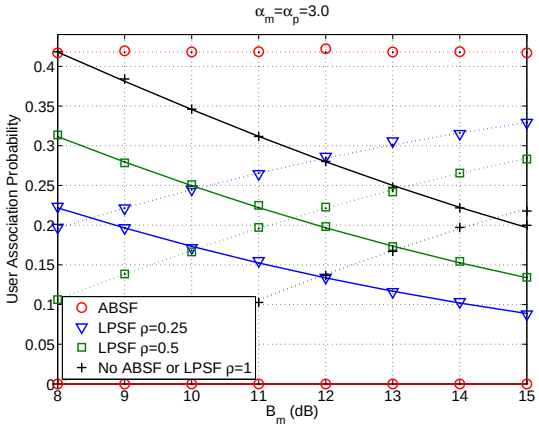

Fig. 2. User association probability of MUEs with various B_m values conditioned on $\lambda_p = 3\lambda_m$

the user group definition in (4), we have the probabilities for the four user groups as follows:

$$\begin{aligned}
&\text{Prob}(pm) = \frac{\lambda_m}{\lambda_m + k_c^2\lambda_p}, \quad \text{Prob}(up) = \frac{k_e^2\lambda_p}{\lambda_m + k_p^2\lambda_p},\\
&\text{Prob}(um) = \frac{\lambda_m\lambda_p(k_c^2 - k_e^2)}{(\lambda_m + k_c^2\lambda_p)(\lambda_m + k_e^2\lambda_p)},\\
&\text{Prob}(pp) = \frac{\lambda_m\lambda_P(k_2^e - k_p^2)}{(\lambda_m + k_e^2\lambda_p)(\lambda_m + k_p^2\lambda_p)}.
\end{aligned} \tag{6}$$

In order to translate the variables k_c and k_e into an analogous form to k_p, we define k_c and k_e with the center region bias B_m and range expansion bias B_p as:

$$k_c = (\frac{B_m P_p}{\rho P_m})^{\frac{2}{\alpha_m+\alpha_p}}, \quad k_e = (\frac{B_p P_p}{P_m})^{\frac{2}{\alpha_m+\alpha_p}}. \tag{7}$$

Therefore, B_p and B_m can be written as

$$B_m = \frac{\rho P_m}{P_p}(k_c)^{\frac{\alpha_m+\alpha_p}{2}}, \qquad B_p = \frac{P_m}{P_p}(k_e)^{\frac{\alpha_m+\alpha_p}{2}}. \tag{8}$$

In a special case, if $\rho = 0$, we define $k_c = \infty$, where its relationships to both k_e and B_m are broken. In that case, the PSFs are configured as the ABSF in the eICIC. The relationship of ρ, B_m, Prob(pm) and Prob(um) conditioned on the same path-loss exponent is shown in Fig. 2, with the optimal value of k_e obtained in Section III. The result illustrates that the probability of the center region PSF MUEs improves (dotted curves) and that of the USF MUEs declines (solid curves with black dots) while the variable B_m increases. The corresponding markers are Monte Carlo simulation results.

B. Distribution of Serving BS Distance

After the users are associated to BSs based on their nearest distance to the BSs in different tiers, next we will discuss the probability distribution function of the serving BS distance.

We consider a typical user served by a BS in the i^{th} tier. The two-dimensional Euclidean distance from the BS is denoted as r_i and the nearest distance from the interfering j^{th} tier BSs is denoted as r_j. Thus, we have the following results regarding the distribution of the serving BS distance.

Lemma 2. *The PDF $f_{r_i}(r)$ of serving BS distance conditioned on $r_j > kr_i$ is*

$$f_{r_i|r_j>kr_i}(r) = 2\pi r(\lambda_i + k^2\lambda_j)\exp\left(-\pi r^2(\lambda_i + k^2\lambda_j)\right). \tag{9}$$

Proof. Using Bayes' rule, we have the probability of $r_i < R$ with condition $r_j > kr_i$:

$$\text{Prob}\left(r_i < R | r_j > kr_i\right) = \frac{\text{Prob}\left(r_i < R, r_j > kr_i\right)}{\text{Prob}\left(r_j > kr_i\right)}. \tag{10}$$

The joint probability could be calculated as follows:

$$\begin{aligned}
&\text{Prob}\left(r_i < R, r_j > kr_i\right)\\
&\overset{(a)}{=} \int_0^R \text{Prob}(r_j > kr_i | r_i = r) f_{r_i}(r) dr\\
&\overset{(b)}{=} 2\pi\lambda_i \int_0^R r\exp(-\lambda_j\pi k^2 r^2)\exp(\lambda_i\pi r^2) dr\\
&= \frac{\lambda_i}{\lambda_i + k^2\lambda_j}\left(1 - \exp(-\pi R^2(\lambda_i + k^2\lambda_j))\right),
\end{aligned} \tag{11}$$

where step (a) follows from the theorem of joint probability function and step (b) is derived from the probability of no point scattering in the region covered with radius kr_i in a PPP. Combining with Lemma 1, we have the conditioned probability result as:

$$\text{Prob}\left(r_i < R | r_j > kr_i\right) = 1 - \exp(-\pi R^2(\lambda_i + k^2\lambda_j)). \tag{12}$$

Then after taking partial derivative with respect to the variable R, we obtain (9). □

Using Lemma 2 and the user group definition (6), we have the PDFs of the serving distances in (13).

III. Coverage Performance Analysis

This section is our main analysis part. We derive the integral form expression of the overall SINR and rate coverage performance with different path-loss exponents. Moreover, under the assumption of the same path-loss exponent, the expression of the rate coverage performance is derived. At the end of this section, the optimal bias values are discussed.

A. Overall SINR Coverage

We define the overall SINR coverage as the probability of SINR larger than a threshold, equivalent to the Complementary Cumulative Distribution Function (CCDF). The overall SINR coverage can be comprehended as the fraction of users who have better SINR than the threshold value. In our analysis, we assume the UEs and BSs are all static as a snapshot scene. Also, a UE can be allocated with either PSFs or USFs only. Then the overall SINR coverage probability $\mathcal{P}_{cov}$ is given as

$$\mathcal{P}_{cov} = \sum_{l\in L} \mathbb{P}_{cov}(l)\text{Prob}(l), \tag{14}$$

$$
\begin{aligned}
f_{pm}(r) =& 2\pi r(\lambda_m + k_c^2\lambda_p)\exp\left(-\pi r^2(\lambda_m + k_c^2\lambda_p)\right)\\
f_{um}(r) =& 2\pi r\frac{(\lambda_m + k_c^2\lambda_p)(\lambda_m + k_e^2\lambda_p)}{\lambda_p(k_c^2 - k_e^2)}\left[\exp\left(-\pi r^2(\lambda_m + k_e^2\lambda_p)\right) - \exp\left(-\pi r^2(\lambda_m + k_c^2\lambda_p)\right)\right]\\
f_{pp}(r) =& 2\pi r\frac{(\lambda_m + k_e^2\lambda_p)(\lambda_m + k_p^2\lambda_p)}{\lambda_m(k_e^2 - k_p^2)}\left[\exp\left(-\pi r^2(\lambda_m/k_e^2\ + \lambda_p)\right) - \exp\left(-\pi r^2(\lambda_m/k_p^2\ + \lambda_p)\right)\right]\\
f_{up}(r) =& 2\pi r(\lambda_m/k_p^2\ + \lambda_p)\exp\left(-\pi r^2(\lambda_m/k_p^2\ + \lambda_p)\right)
\end{aligned}
\tag{13}
$$

where $\mathbb{P}_{cov}(l)$ is the common expression of overall SINR coverage of a typical UE. It can be further represented as follows:

$$
\begin{aligned}
&\mathbb{P}_{\text{cov}}(l) = \mathbb{P}_{\text{cov}}\left(\Phi_l > \tau\right)\\
&= \mathbb{E}\left[\text{Prob}\left(\frac{\rho_l P_l h r^{-\alpha_l}}{{\rho'}_l I_{M_l} + I_{P_l} + \sigma^2} > \tau\,|r\right)\right]\\
&= \int_R \mathbb{E}_I\left[\text{Prob}\left(h > \frac{\tau r^{\alpha_l}}{\rho_l P_l}({\rho'}_l I_{M_l} + I_{P_l} + \sigma^2)\right)\right] f_l(r)dr\\
&\overset{(a)}{=} \int_R \mathbb{E}_I\left[\exp\left(\mu\frac{\tau r^{\alpha_l}}{\rho_l P_l}({\rho'}_l I_{M_l} + I_{P_l} + \sigma^2\right)\right] f_l(r)dr\\
&= \int_R \exp\left(\mu\frac{\tau r^{\alpha_l}}{\rho_l P_l}\sigma^2\right)\mathbb{E}_{I_{M|l}}\cdot\mathbb{E}_{I_{P|l}}\cdot f_l(r)dr,
\end{aligned}
\tag{15}
$$

where step (a) is derived from the CDF of exponential distribution h. The macro aggregate interference $\mathbb{E}_{I_{M|l}}$ and the pico aggregate interference $\mathbb{E}_{I_{P|l}}$ can be further written as:

$$
\begin{aligned}
\mathbb{E}_{I_{M|l}} =& \mathbb{E}_{h,x}\left[\exp\left(-\frac{\mu\tau r^{\alpha_l}{\rho'}_l}{\rho_l P_l}\sum_{m\in M_l} P_m h_m {x_m}^{-\alpha_l}\right)\right],\\
\mathbb{E}_{I_{P|l}} =& \mathbb{E}_{h,x}\left[\exp\left(-\frac{\mu\tau r^{\alpha_l}{\rho'}_l}{\rho_l P_l}\sum_{n\in P_l} P_p h_n {x_n}^{-\alpha_p}\right)\right].
\end{aligned}
\tag{16}
$$

As the open access mode is employed, it is worth highlightening that the nearest interfering distance has its lower limit. In order to calculate the aggregate interference, we have the following result concerning the interference from the i^{th} tier.

Lemma 3. *The Laplace transform $\mathcal{L}_{I_i}(s)$ of the aggregate interference from the i^{th} tier is*

$$
\mathcal{L}_{I_i}(s) = \exp\left(-\pi\lambda_i(\frac{sP_i}{\mu})^{\frac{2}{\alpha_i}}C((kr)^{\alpha_i}(\frac{s}{\mu})^{-1},\alpha_i)\right), \tag{17}
$$

where function $C(a,b)$ is

$$
C(a,b) \approx \begin{cases} A(b) - a^{2/b}\left(1 - \dfrac{2a}{b+2}\right), a < 1 \\ B(b)a^{2/b-1}\left(1 - \dfrac{(b-2)a^{-1}}{2b-2}\right), a \geq 1 \end{cases}. \tag{18}
$$

Proof. See Appendix B. □

The functions $A(b)$ and $B(b)$ are defined as follows, and the function $\Gamma(\cdot)$ is the Gamma function.

$$
A(b) = \int_0^\infty (1 + x^{b/2})^{-1}dx \quad B(b) = -\frac{2\Gamma(2/b-1)}{b\Gamma(2/b)} \tag{19}
$$

If the interference and signal are both from the same tier, the minimum interfering distance is simplified as r with $k = 1$. For simplicity, we assume the thermal noise is approximately zero ($\sigma \sim 0$), which has negligible effect on the final results [5], referred as the interference limited network [16].

Equipped with Lemma 3, and $\mathbb{E}[\exp(-sI_i)] = \mathcal{L}_{I_i}(s)$, we have the following result regarding the overall SINR coverage of a typical UE in our network scenario as:

Theorem 1. *The SINR coverage of a typical UE following the user association strategy in* (4) *is given in* (20) *at the top of next page.*

Proof. Combining Lemma 3 with (15) and (16), we have the result. □

In (20), $\hat{P_m} = P_m/P_p$ and $D(\lambda,\alpha,t,\tau) = r^2\lambda\tau^{\frac{2}{\alpha}}C(\tau^{-1},\alpha)$. Moreover, the exponential part of the integration in each equation is obtained by the Laplace transform of the aggregate interference from both tiers. Then we obtain the expectation value of coverage probability averaged on the serving distance r of the exponential part, which is the SINR coverage. With these results, we have the overall SINR coverage following (14). The closed-form result can be obtained when the macro-cells and pico-cells have the same path-loss exponent (α_m=α_p). Otherwise, we evaluate the result numerically.

B. Rate Coverage

Similar to the overall SINR analysis, the common expression of the rate coverage probability Prob$(R_l > \omega)$ is defined as:

$$
\text{Prob}(R_l > \omega) = \text{Prob}\left(\frac{\beta_l W}{N_l}\log_2(1 + \Phi_l) > \omega\right), \tag{21}
$$

where ω is the threshold of the downlink throughput and Φ_l denotes the SINR of the user group l. It can be comprehended as the average fraction of users achieving a target rate. In order to obtain the expectation of variable N_l, we have the following results with the assumption of an i.i.d PPP deployment of UEs with density λ_u.

Lemma 4. *The expectation of the UE number $\mathbb{E}(N)$ in a Voronoi macro-cell is λ_u/λ_m.*

Proof. See Appendix C. □

$$
\begin{aligned}
\mathbb{P}_{cov}(pm) &= \int_0^\infty \left[\exp\left(-\pi\left(D(\lambda_m,\alpha_m,r,\tau)+\lambda_p r^{\frac{2\alpha_m}{\alpha_p}}(\tau(\hat{P_m}\rho)^{-1})^{\frac{2}{\alpha_p}}C(k_c{}^{\alpha_p}r^{\alpha_p-\alpha_m}\rho\hat{P_m}\tau^{-1},\alpha_p)\right)\right)\right] f_{pm}(r)dr\\
\mathbb{P}_{cov}(um) &= \int_0^\infty \left[\exp\left(-\pi\left(D(\lambda_m,\alpha_m,r,\tau)+\lambda_p r^{\frac{2\alpha_m}{\alpha_p}}(\tau\hat{P_m}^{-1})^{\frac{2}{\alpha_p}}C(k_e{}^{\alpha_p}r^{\alpha_p-\alpha_m}\hat{P_m}\tau^{-1},\alpha_p)\right)\right)\right] f_{um}(r)dr\\
\mathbb{P}_{cov}(pp) &= \int_0^\infty \left[\exp\left(-\pi\left(D(\lambda_p,\alpha_p,r,\tau)+\lambda_m r^{\frac{2\alpha_p}{\alpha_m}}(\tau\rho\hat{P_m})^{\frac{2}{\alpha_m}}C(k_e{}^{-\alpha_m}r^{\alpha_m-\alpha_p}(\tau\rho\hat{P_m})^{-1},\alpha_m)\right)\right)\right] f_{pp}(r)dr\\
\mathbb{P}_{cov}(up) &= \int_0^\infty \left[\exp\left(-\pi\left(D(\lambda_p,\alpha_p,r,\tau)+\lambda_m r^{\frac{2\alpha_p}{\alpha_m}}(\tau\hat{P_m})^{\frac{2}{\alpha_m}}C(k_p{}^{-\alpha_m}r^{\alpha_m-\alpha_p}(\tau\hat{P_m})^{-1},\alpha_m)\right)\right)\right] f_{up}(r)dr
\end{aligned}
\tag{20}
$$

Combining the Lemma 4 with user association probabilities in (6), then the four group average served UE numbers are as follows:

$$
\begin{aligned}
&\mathbb{E}(N_{pm}) = \frac{\lambda_u}{\lambda_m + k_c^2\lambda_p}, \quad \mathbb{E}(N_{up}) = \frac{k_p^2\lambda_p\lambda_u}{{\lambda_m}^2 + k_p^2\lambda_m\lambda_p},\\
&\mathbb{E}(N_{um}) = \frac{\lambda_u\lambda_p(k_c^2-k_e^2)}{(\lambda_m+k_c^2\lambda_p)(\lambda_M+k_e^2\lambda_p)},\\
&\mathbb{E}(N_{pp}) = \frac{\lambda_u\lambda_P(k_e^2-k_p^2)}{(\lambda_m+k_e^2\lambda_p)(\lambda_M+k_p^2\lambda_p)}.
\end{aligned}
\tag{22}
$$

Equipped with the expectaion results of UE numbers in (22), we have the following result regarding the rate coverage probability:

Theorem 2. *The common expression of rate coverage probability* $\mathbb{R}_{cov}(l)$ *is*

$$
\mathbb{R}_{cov}(l) = \mathbb{P}_{cov}(l)\big|_{\tau=t\left(\frac{\omega\mathbb{E}(N_l)}{\beta_l W}\right)}. \tag{23}
$$

Proof. From (21), the equation can be translated into the following result:

$$
\mathbb{R}_{cov}(l) = \mathbb{E}_{N_l}\left[\text{Prob}\left(\Phi_l > 2^{\frac{\omega N_l}{\beta_l W}}-1\right)\right]. \tag{24}
$$

It is the same as the SINR coverage probability. By substituting 2^x-1 with $t(x)$, we have the following:

$$
\mathbb{E}_{N_l}\left[\mathbb{P}_{cov}(l)\big|_{\tau=t\left(\frac{\omega N_l}{\beta_l W}\right)}\right]. \tag{25}
$$

However, equation (25) is difficult to calculate. Thus we get the approximation value by exchanging the calculation order of the expectation and the integration following from [7] as in step (a).

$$
\begin{aligned}
\mathbb{R}_{cov}(l) &= \mathbb{E}_{N_l}\left[\text{Prob}\left(\Phi_l > 2^{\frac{\omega N_l}{\beta_l W}}-1\right)\right]\\
&= \mathbb{E}_{N_l}\left[\mathbb{P}_{cov}(l)\big|_{\tau=t\left(\frac{\omega N_l}{\beta_l W}\right)}\right]\\
&\overset{(a)}{\approx} \mathbb{P}_{cov}(l)\big|_{\tau=t\left(\frac{\omega\mathbb{E}(N_l)}{\beta_l W}\right)}.
\end{aligned}
\tag{26}
$$

□

Combining Theorem 2 with the user number expectations in (22), we have the rate coverage results of each group. Thus the overall rate coverage probability can be calculated by $\sum_l \text{Prob}(l)\mathbb{R}_{cov}(l)$. Similar to the SINR analysis, this result has a closed form expression in (27) when $\alpha_m = \alpha_p \equiv \alpha$. It represents the fraction of the users in the whole network have a larger throughput than the threshold. For denotation simplicity, we use the following parameters which is shown in TABLE I, where $l \in L\{cm, um, cp, up\}$. If the path-loss exponents are different, the result is analysed numerically.

TABLE I
ABBREAVATIONS IN Ω

Parameter	Value
t_l	$t\left(\frac{\omega\mathbb{E}(N_l)}{\beta_l W}\right)$
e_l	$t_l{}^{\frac{2}{\alpha}}C(t_l{}^{-1},\alpha)+1$
f_l	$\hat{P_m}(\rho_l' t_l)^{-1}$
f_l'	$(\hat{P_m}\rho_l' t_l)^{-1}$

C. Optimal Bias Values

Under the assumption $\alpha_m = \alpha_p \equiv \alpha$, the optimal bias values of k_c and k_e can be written as the following form to maximize the overall rate coverage probability:

$$
[k_c{}^{opt}, k_e{}^{opt}] = \arg\max_{k_c,k_e}\{\Omega(k_c,k_e)\}. \tag{28}
$$

As the biases B_m and B_p always have upper and lower limits, the values of k_c and k_e also have limited ranges according to (7). Moreover, as the terms f_l and e_l include both k_c and k_e, the objective function is too complicated to obtain a closed-form optimised value. Thus the optimal values of k_c and k_e can only be analysed numerically. However, the procedure is exhaustive because of the two-dimensional search space. In order to reduce the time and resource for searching, we proposed a new method to obtain the near optimal values by a single iteration method. The main idea is translating the search space into several one-dimension spaces. In the following, first we propose a near optimal value for k_c related to k_e based on the SINR property of the PSF MUEs and the USF MUEs. Then we substitute the value of k_c with this k_e-related value in (28) to have the near optimal value of k_e. Eventually the near optimal value of k_c is calculated with the substitution of the near optimal value of k_e in (28). The details of the single-iteration method are given below.

When considering the effect of k_c on the macro-cell, we treat the value of k_e as a constant. As a result, the number of the MUEs is determined, denoted as N_{mue}. Then the

$$\Omega = \left\{ \frac{1}{\theta k_c^2 + \theta {f_{pm}}^{-\frac{2}{\alpha}} C(f_{pm} k_c^{\alpha}, \alpha) + e_{pm}} + \frac{1}{\theta k_e^2 + \theta {f_{um}}^{-\frac{2}{\alpha}} C(f_{um} k_e^{\alpha}, \alpha) + e_{um}} - \frac{1}{\theta k_c^2 + \theta {f_{um}}^{-\frac{2}{\alpha}} C(f_{um} k_e^{\alpha}, \alpha) + e_{um}} + \frac{1}{\theta^{-1} k_e^{-2} + \theta^{-1} {f'_{pp}}^{-\frac{2}{\alpha}} C(f'_{pp} k_e^{-\alpha}, \alpha) + e_{pp}} - \frac{1}{\theta^{-1} k_p^{-2} + \theta^{-1} {f'_{pp}}^{-\frac{2}{\alpha}} C(f'_{pp} k_p^{-\alpha}, \alpha) + e_{pp}} + \frac{1}{\theta^{-1} k_p^{-2} + \theta^{-1} {f'_{up}}^{-\frac{2}{\alpha}} C(f'_{up} k_p^{-\alpha}, \alpha) + e_{up}} \right\} \tag{27}$$

maximum rate coverage probability problem is formulated as a maximum minimum rate performance problem, denoted as

$$\begin{aligned} &\max_{N_l} \{\min\{R_{um}, R_{pm}\}\} \\ &s.t. \quad N_{um} + N_{pm} = N_{mue}. \end{aligned} \tag{29}$$

Without the explicit SINR values, this problem is difficult to resolve. Fortunately, if we assume the overall SINR of the PSF MUEs is identical to that of the USF MUEs, the maximum coverage probability is achieved when following the relationship of user association probabilities of the PSF MUEs and the USF MUEs:

$$\frac{\text{Prob}(pm)}{\text{Prob}(um)} = \frac{\beta}{1-\beta}. \tag{30}$$

For denotation simplicity, we replace β' with $\frac{\beta}{1-\beta}$. Furthermore, combining (30) with the user association probability in (6), we have the following relationship of k_c and k_e as:

$$k'_c = \sqrt{{k_e}^2 + \frac{\lambda_m + {k_e}^2 \lambda_p}{\lambda_p \beta'}}. \tag{31}$$

As the allocating resource contributes more than the SINR when the optimal rate coverage is obtained intuitively, the value of k'_c can be deemed as the initial near optimal value of k_c. Equipped with this k'_c, the near optimal k_e, denoted as $\hat{k}_e^{opt}$ can be evaluated numerically by (32). It is because the first term and last term in (27) exclude variable k_e.

$$\hat{k}_e^{opt} = \arg\max_{k_c = k'_c, k_e} \left[\frac{1}{\theta k_e^2 + \theta {f_{um}}^{-\frac{2}{\alpha}} C(f_{um} k_e^{\alpha}, \alpha) + e_{um}} - \frac{1}{\theta k_c^2 + \theta {f_{um}}^{-\frac{2}{\alpha}} C(f_{um} k_e^{\alpha}, \alpha) + e_{um}} + \frac{1}{\theta^{-1} k_e^{-2} + \theta^{-1} {f'_{pp}}^{-\frac{2}{\alpha}} C(f'_{pp} k_e^{-\alpha}, \alpha) + e_{pp}} - \frac{1}{\theta^{-1} k_p^{-2} + \theta^{-1} {f'_{pp}}^{-\frac{2}{\alpha}} C(f'_{pp} k_p^{-\alpha}, \alpha) + e_{pp}} \right]. \tag{32}$$

Therefore, by combining the value of ${k_e}^{opt}$ with (28), the near optimal value of k_c, $\hat{k}_c^{opt}$, can also be obtained numerically by the following result.

$$\hat{k}_1^{opt} = \arg\max_{k_c, k_e = \hat{k}_2^{opt}} \left[\frac{1}{\theta k_c^2 + \theta {f_{pm}}^{-\frac{2}{\alpha}} C(f_{pm} k_c^{\alpha}, \alpha) + e_{pm}} - \frac{1}{\theta k_c^2 + \theta {f_{um}}^{-\frac{2}{\alpha}} C(f_{um} k_e^{\alpha}, \alpha) + e_{um}} \right]. \tag{33}$$

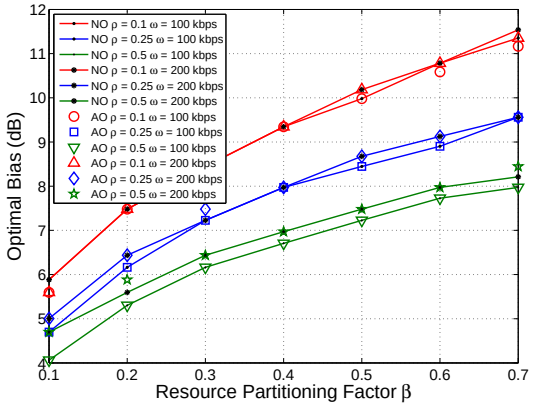

Fig. 3. Optimal range expansion bias with varieties of power reduction factor ρ, and rate threshold $\omega = 100$ and 200 kbps

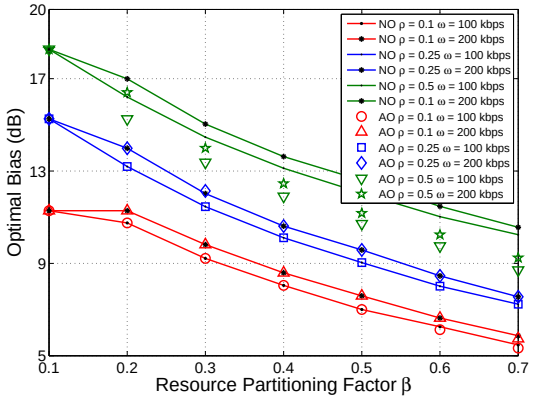

Fig. 4. Optimal center region bias with varieties of ρ, and rate threshold $\omega = 100$ and 200 kbps

Thus the near optimal values of k_c and k_e are obtained by this single iteration method. Interestingly, the near optimal values are very close to the actually numerical optimal results when the search of the optimal k_e starts with k_c in (31). Equipped with these optimal values and the definition of B_p and B_m in (8), the comparison of the near optimal values and the actual optimal values is illustrated in Fig. 3 and Fig. 4.

Fig. 3 shows the actual optimal (AO) value and near optimal (NO) value of B_p with two rate thresholds (100 and 200 kbps respectively). On one hand, the gap between them is negligible. It proves the effectiveness of our proposed single iteration method. On the other hand, the optimal B_p increases

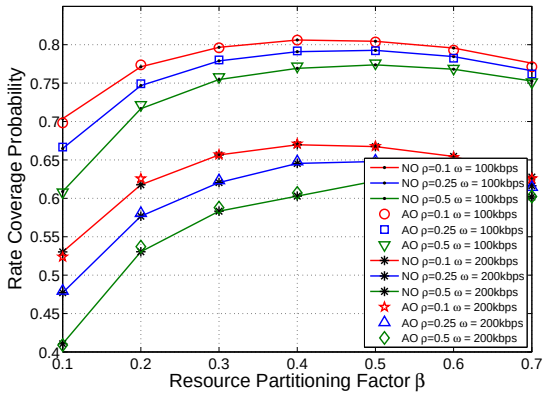

Fig. 5. Rate coverage in terms of the near optimal and actual optimal biases

with the resource partitioning factor β. The increasing value of β provides more PSF resources and less USF resources, resulting in that the PSF PUEs outperform the USF MUEs in average throughput. Therefore, the average rate coverage probability can be improved by extending the pico-cell expansion region. The comparison between the proposed near optimal and actual optimal B_m is illustrated in Fig. 4, also with two rate thresholds (100 and 200 kbps respectively). The results show that when the power reduction factor ρ is small (0.1 and 0.25), the difference between these two optimal biases in terms of B_m is negligible. However, with the increase of the power level of the LPSF (0.5), the gap between them increases but never exceeds 2 dB. As shown in the rate coverage performance comparison in Fig. 5, this gap contributes so little that the coverage performances of the near optimal and actual optimal results are almost the same. The reason is that the small offset on B_m has negligible effect on the rate coverage performance when the bias B_m is relatively large, resulting from the relatively higher transmitting power of the LPSF. Therefore, it is reasonable to consider the value achieved from the single iteration method as the near optimal value.

IV. Numerical Results and Discussion

In this section we present the numerical results of the overall SINR coverage probability and the rate probability derived in Section III and validate the results with Monte Carlo simulation. Furthermore, the effect of the power reduction factor and resource partitioning factor on the SINR and the rate coverage performance is studied through the numerical results. The simulated network coverage area is assumed to be a square area of 5000m $\times$ 5000m. We sample 10000 times where BSs are deployed following the PPP model and the UE is deployed at the origin. The simulation parameters are summarized in Table II.

In Fig. 6, we compare the overall SINR coverage performance with different path-loss exponents. The Monte Carlo simulation results match the numerical results, especially when the macro and pico cell path-loss exponents are equal. It proves the effectiveness of our model. Moreover, the system

TABLE II
NOTATIONS AND PARAMETERS

Parameter	Description	Value
$\mathcal{S}$	Square Range	$5000 \times 5000\ m^2$
W	Spectrum Bandwidth	5 MHz
λ_m	Density of MBS	$1.27e^{-6}\ /m^2$
λ_p	Density of PBS	$3\lambda_m$
λ_u	Density of UEs	$30\lambda_m$
P_m	Maximum Power of MBS	43 dB
P_p	Maximum Power of PBS	30 dB
α_m	Macrocell Path-loss Exponent	2.5 and 3.0
α_p	Picocell Path-loss Exponent	2.5 and 3.0
β	Resource Partitioning Factor	0.5
μ	Exponential Distribution Factor	1
k_c	Center Region Factor	${k_c}^{opt}$
k_e	Range Expansion Factor	${k_e}^{opt}$
k_p	Picocell Coverage Factor	$(\frac{P_p}{P_m})^{\frac{2}{\alpha_m+\alpha_p}}$
B_m	Center Region Bias ($\rho \neq 0$)	$\frac{\rho P_m}{P_p}(k_c)^{\frac{\alpha_m+\alpha_p}{4}}$
B_p	Range Expansion Bias	$\frac{P_m}{P_p}(k_e)^{\frac{\alpha_m+\alpha_p}{4}}$

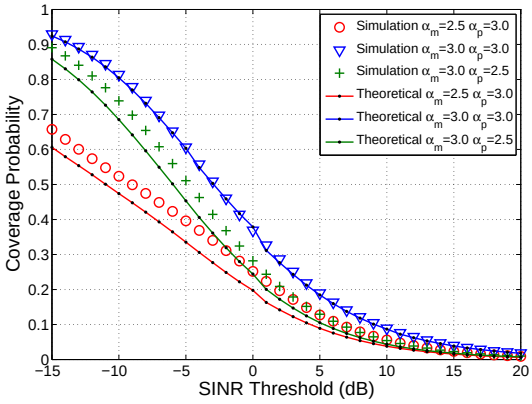

Fig. 6. Overall SINR performance with different path-loss exponents

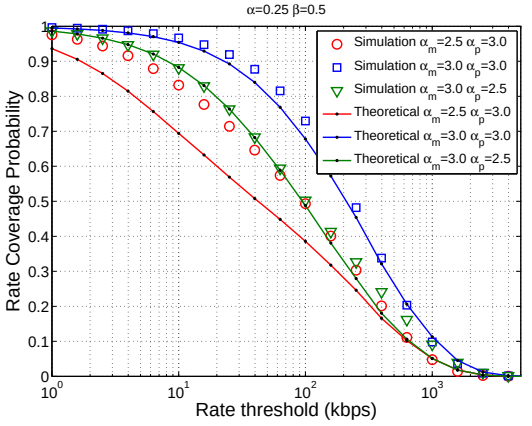

Fig. 7. Overall rate coverage performance with different path-loss exponents

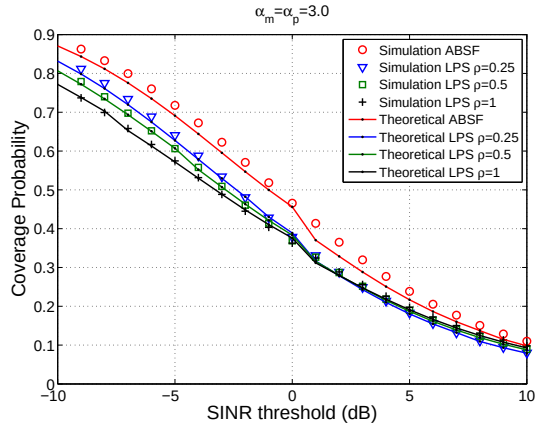

Fig. 8. Overall SINR performance with different power reduction factors

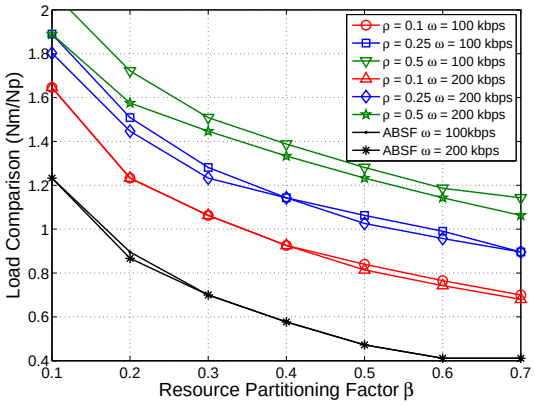

Fig. 10. Load compasison with variety of β in terms of the optimal biases

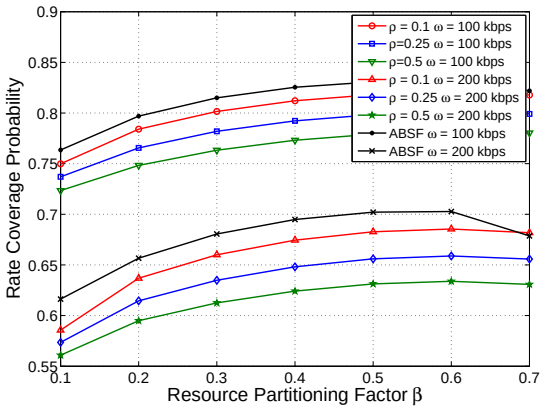

Fig. 9. Overall rate coverage with varieties of β in terms of optimal biases

with lower pico-cell path-loss exponent outperforms the one with lower macro-cell path-loss exponent on overall SINR coverage performance. This has two causes. The first cause is the technique of the pico-cell range expansion. When the macro-cell has lower path-loss exponent, then the cell range expansion users suffer stronger interference from the macro BSs. Also, with relatively higher path-loss exponent of the pico-cell, the users receive weaker signals. The second cause is that the macro BS has a higher transmitter power. Under the same circumstance, the macro BS causes higher interference than the pico BS.

Fig. 7 shows the overall rate coverage probability with different path-loss exponents as in Fig. 6. Similar to the SINR results, the numerical results (solid curves with black dots) closely match the Monte Carlo simulation (only markers), especially when the path-loss exponents are the same.

In Fig. 8, we compare the overall SINR coverage performance of different LPSF power. It shows that the ABSF has better SINR performance than the LPSF. As the cell range expansion users suffer no interference from the macrocell on the data transmission when applying the ABSF, it always has a better SINR than the LPSF, which degrade the cell range expansion users' SINR. Also, the LPSF also degrades the SINR of the macrocell center region. Thus the ABSF outperforms the LPSF in the overall SINR coverage. Moreover, for small SINR threshold ($\tau < 0$), as the power reduction factor increases, the performance declines. The SINR deterioration is caused by the increasing interference from the macro BS. On the other hand, for large SINR thresholds, there is nearly no difference with different LPSF power except for the ABSF. The reason is that the average coverage performance in the CRE is poor. When the SINR threshold $\tau > 5$, the overall SINR coverage is approximately zero. Therefore, with the increase of the LPSF power, the performance increases because of the improved PSF MUE performance.

Fig. 9 illustrates the simulated rate coverage probability using the optimal B_m and B_p, in terms of several typical values of the power reduction factor ρ and rate threshold ω. As shown in this figure, the best coverage probability is always achieved when the resource partitioning factor β is approximately 0.6. Moreover, the overall rate coverage yields the best performance when using the ABSF. In the ABSF case, the cell range expansion UEs have the best SINR than the others as they suffer no interference from the macro BSs. Thus, a larger expansion area results in more users having better SINR and rate. However, this causes that more UEs are attracted to the pico-cells, as shown in Fig. 10. It illustrates the ratio between the number of macro-cell and pico-cell UEs per-cell when the optimal rate coverage probability is achieved. The ABSF always have more UEs associated with the pico BSs than the LPSF. This means a heavier burden on the back-haul of the pico-cell. However, in practice, the pico-cell may have a limited back-haul while the macro-cell can be assumed unlimited. These optimal biases for a limited back-haul of the pico-cell are not our focus in this work. In the following, we investigate the rate coverage performance with some typical fixed cell range expansion biases B_p.

In Fig. 11, we compare the overall rate coverage with a variety of resource partitioning factor β, in terms of some typical range expansion biases B_p (3 dB, 7 dB and 12 dB). The rate threshold is set as 100 and 200 kbps respectively. The results show that the two different rate thresholds have similar results. Moreover, different from the results with optimal biases, the rate coverage performance of the LPSF is better than that of the ABSF. On one hand, when the cell range

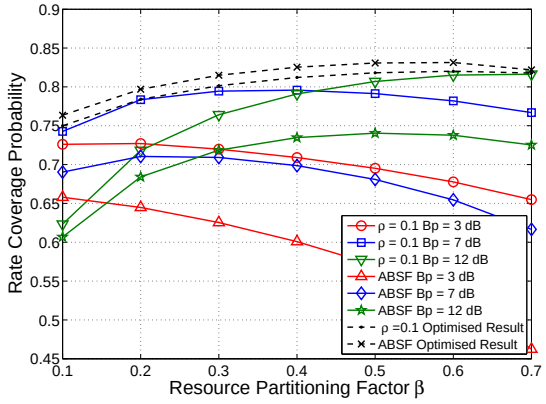

Fig. 11. Overall rate coverage with varieties of β in terms of fixed B_p with $\omega = 100$ kbps

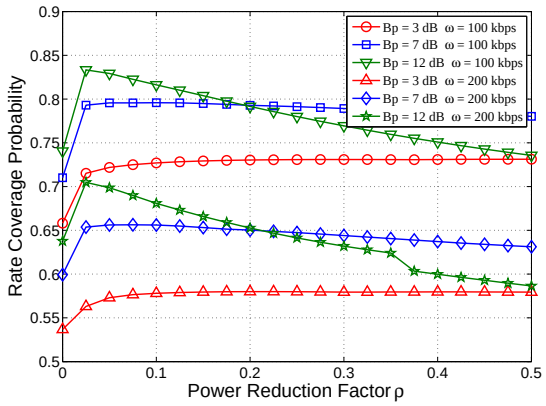

Fig. 12. Overall rate coverage with varieties of ρ

expansion bias is static, in particular when it is small, the LPSF with a relative low power have limited effects on the rate performance of the cell range expansion users. On the other hand, the rate of the edge macro-cell users increases by sharing more spectrum resources.

In Fig. 12, the rate performance is analysed with a variety of power reduction factor ρ, with the typical values of range expansion bias B_p and rate threshold ω. On one hand, the result shows that a sharp increase occurs when the ρ varies from 0. Intuitively, compared with the ABSF, the LPSF provide better rate coverage for the macro-cell edge users by sharing more spectrum, but worse rate coverage for the cell range expansion users. In our case, the transmitting power of the LPSF is low, thus the rate coverage gain in the macro-cells exceeds the loss in the pico-cells, which results in the sharp increase of the overall rate coverage performance. On the other hand, interestingly the performance remains almost constant with various ρ ($\rho \neq 0$) values when the range expansion bias B_p is relatively low. In such a low B_p case, the number of the CRE UEs is small, and by allocating some more resources to these UEs, the rate coverage loss due to their degraded SINR is made up. In other words, by adjusting the resource partitioning factor β, the coverage performance is not affected by power reduction ρ when the range expansion bias is low (under 7 dB in our simulation). However, a larger range expansion bias results in more UEs to camp to the pico-cell in its expansion region, which will be significantly interfered when the transmitting power of the LPSF is large. Therefore, the coverage performance declines with the increase of the power reduction factor ρ when the range expansion bias is large.

V. Conclusion

In this paper we have obtained the analytical results to calculate the overall SINR and rate coverage performance employing the LPSF in the FeICIC. Following the results, the overall rate coverage performance is analysed with the biases, the power reduction factor and the resource partitioning factor. We conclude that with the optimal center and cell range expansion biases, the ABSF outperform the LPSF in terms of both SINR and rate coverage. As the ABSF scheme has a larger optimal CRE bias, more UEs will be attracted to the CRE regions. This will result in a heavier back-haul burden on the pico-cells, which in practice may have limited back-haul capability. The impact of limited back-haul on HetNet performance will be studied in our future work. Moreover, if the range expansion bias is static and not optimal, the LPSF in turn outperform the ABSF in terms of rate coverage performance, by sharing more spectrum resource in the macro-cell edge region. Furthermore, when the cell range expansion bias is relatively low (under 7 dB), the power reduction factor has negligible effect on the rate coverage when the resource partition factor is adjusted.

Acknowledgement

This paper acknowledges the support of the MOST of China for the "Small Cell and Heterogeneous Network Planning and Deployment" project (No. 2015DFE12820), the WiNDOW research project supported by the European Commission under its 7th Framework Program (No. 318992), the National Natural Science Foundation of China (No. 61571073), the National High Technology Research and Development Program of China (No. 2014AA01A701), and the China Scholarship Council(CSC). Also, we would like to thank the anonymous reviewers whose constructive and detailed comments helped us a lot to improve the quality of this paper.

Appendix A
Proof of Lemma 1

Firstly, the PDF of two-point distance $f_{r_j}(r)$ in PPP is $2\pi\lambda_j r \exp(-\pi\lambda_j r^2)$ [5]. Prob$(r_i > kr_j)$ could be comprehended as the probability, for an arbitrary point in Θ_i, of no point is closer than kr_j. Then the expression is given as

$$\begin{aligned}
&\text{Prob}(r_i > kr_j) \\
&= \text{Prob}\{\text{no point closer than } kr_j | r_j\} \\
&= \int_0^\infty \exp(-\lambda_i \pi k^2 r^2) f_{r_j}(r) dr \\
&= 2\pi\lambda_j \int_0^\infty \exp(-\pi r^2(\lambda_i k^2 + \lambda_j)) r dr \\
&= \frac{\lambda_j}{\lambda_j + k^2\lambda_i}.
\end{aligned} \tag{34}$$

APPENDIX B
PROOF OF LEMMA 3

The Laplace transform $\mathcal{L}_{I_i}(s)$ of the aggregate interference I_i with distance larger than kr is given as:

$$\begin{aligned}
&\mathcal{L}_{I_i}(s) = \mathbb{E}(\exp(-sI_i)) \\
&= \mathbb{E}\left(\prod_{i|r_i>kr} \exp(-sP_i h r_i^{-\alpha_i})\right) \\
&\overset{(a)}{=} \exp\left(-2\pi\lambda_i \int_{kr}^{\infty} (1 - \mathbb{E}_h\left[\exp(-sP_i h u^{-\alpha_i})\right]) u du\right) \\
&\overset{(b)}{=} \exp\left(-2\pi\lambda_i \int_{kr}^{\infty} \frac{sP_i u^{-\alpha_i}}{sP_i u^{-\alpha_i} + \mu} u du)\right) \\
&\overset{(c)}{=} \exp\left(-\pi\lambda_i (\frac{sP_i}{\mu})^{\frac{2}{\alpha_i}} \int_{(kr)^2(\frac{sP_i}{\mu})^{\frac{-2}{\alpha_i}}}^{\infty} \frac{1}{1+t^{\frac{\alpha_i}{2}}} dt\right) \\
&= \exp\left(-\pi\lambda_i (\frac{sP_i}{\mu})^{\frac{2}{\alpha_i}} C((kr)^{\alpha_i} (\frac{sP_i}{\mu})^{-1}, \alpha_i)\right),
\end{aligned} \tag{35}$$

where step (a) follows from the probability generating functional of the PPP and step (b) is derived by $h \sim \exp(\mu)$. Then given $t = (\mu/sP_i)^{2/\alpha_i} u^2$, we get (c). Thus by implying $C(a,b) = \int_{a^{2/b}}^{\infty} 1/(1+t^{b/2}) dt$, the result is obtained. Next, in order to numerically evaluate our expression, the approximation of $C(a,b)$ is investigated in terms of a. On one hand, for small parameter ($a < 1$), the expression can be given as

$$\begin{aligned}
C(a,b) &= \int_0^{\infty} 1/(1+t^{b/2}) dt - \int_0^{a^{2/b}} 1/(1+t^{b/2}) dt \\
&\overset{(a)}{=} A(b) - t \cdot {}_2F_1\left(1, \frac{2}{b}; 1+\frac{2}{b}; -t^{\frac{b}{2}}\right)\Big|_0^{a^{2/b}} \\
&\overset{(b)}{\approx} A(b) - a^{2/b}\left(1 - \frac{2a}{b+2}\right),
\end{aligned} \tag{36}$$

where $A(b) = \int_0^{\infty} (1+x^{b/2})^{-1} dx$ and ${}_2F_1(\cdot)$ is the Gauss hypergeometric function. Step (a) is calculated by the symbolic integral calculator [17] and step (b) is the first order series expansion of the Gauss hypergeometric function. The smaller the parameter a the closer match to the actual value.
On the other hand, when a is large ($a \geq 1$), we can approximate the result as

$$\begin{aligned}
C(a,b) &\overset{(a)}{=} t \cdot {}_2F_1\left(1, \frac{2}{b}; 1+\frac{2}{b}; -t^{\frac{b}{2}}\right)\Big|_{a^{2/b}}^{\infty} \\
&\overset{(b)}{=} B(b) a^{(2/b-1)} {}_2F_1(1, 1-\frac{2}{b}; 2-\frac{2}{b}; a^{-1}) \\
&\overset{(c)}{\approx} B(b) a^{(2/b-1)}\left(1 - \frac{(b-2)a^{-1}}{2b-2}\right),
\end{aligned} \tag{37}$$

where

$$B(b) = -\frac{2\Gamma(2/b-1)}{b\Gamma(2/b)}. \tag{38}$$

Step (a) is calculated by the symbolic integral calculator [17] and step (b) is achieved by combining (a) in (37) with (9) in [18]. Step (c) follows from the first order series expansion of the Gauss hypergeometric function.

APPENDIX C
PROOF OF LEMMA 4

From [19], we have the probability mass function of UE number in a macro-cell as

$$\mathrm{P}(N=n) = \frac{3.5^{3.5}\Gamma(n+3.5)(\lambda_u/\lambda_m)^n}{\Gamma(3.5)n!(\lambda_u/\lambda_m+3.5)^{n+3.5}}. \tag{39}$$

Then using theorem of discrete expectation, the UE number expectation is

$$\begin{aligned}
\mathbb{E}(N) &= \mathbb{E}\left(\mathrm{P}(N=n)\right) \\
&= \sum_{n=1}^{\infty} \frac{3.5^{3.5}\Gamma(n+3.5)(\lambda_u/\lambda_m)^n}{\Gamma(3.5)(n-1)!(\lambda_u/\lambda_m+3.5)^{n+3.5}}.
\end{aligned} \tag{40}$$

For notation simplicity, use x denotes $\frac{\lambda_u/\lambda_m}{\lambda_u/\lambda_m+3.5}$, then this original expression can be presented as follows:

$$\begin{aligned}
\mathbb{E}(N) &= \frac{(1-x)^{3.5}}{\Gamma(3.5)} \sum_{n=1}^{\infty} \frac{\Gamma(n+3.5)}{(n-1)!} x^n \\
&\overset{(a)}{=} \frac{(1-x)^{3.5}}{\Gamma(3.5)} \frac{105 \cdot \pi^{0.5} x}{16(1-x)^{4.5}} \\
&= \lambda_u/\lambda_m,
\end{aligned} \tag{41}$$

where step (a) is calculated in Matlab by serial summarize function.

REFERENCES

[1] A. Damnjanovic, J. Montojo, Y. Wei, T. Ji, T. Luo, M. Vajapeyam, T. Yoo, O. Song, and D. Malladi, "A survey on 3GPP heterogeneous networks," *Wireless Communications, IEEE*, vol. 18, no. 3, pp. 10–21, June 2011.

[2] D. Lopez-Perez, I. Guvenc, G. de la Roche, M. Kountouris, T. Quek, and J. Zhang, "Enhanced intercell interference coordination challenges in heterogeneous networks," *Wireless Communications, IEEE*, vol. 18, no. 3, pp. 22–30, June 2011.

[3] Panasonic, "Performance study on ABS with reduced macro power," 3GPP TSG-RAN WG1, Tech. Rep., Nov 2011.

[4] B. Soret and K. Pedersen, "Macro transmission power reduction for hetnet co-channel deployments," in *Global Communications Conference (GLOBECOM), 2012 IEEE*, Dec 2012, pp. 4126–4130.

[5] J. Andrews, F. Baccelli, and R. Ganti, "A tractable approach to coverage and rate in cellular networks," *Communications, IEEE Transactions on*, vol. 59, no. 11, pp. 3122–3134, November 2011.

[6] H.-S. Jo, Y. J. Sang, P. Xia, and J. Andrews, "Heterogeneous cellular networks with flexible cell association: A comprehensive downlink SINR analysis," *Wireless Communications, IEEE Transactions on*, vol. 11, no. 10, pp. 3484–3495, October 2012.

[7] S. Singh, H. Dhillon, and J. Andrews, "Offloading in heterogeneous networks: Modeling, analysis, and design insights," *Wireless Communications, IEEE Transactions on*, vol. 12, no. 5, pp. 2484–2497, May 2013.

[8] S. Singh and J. Andrews, "Joint resource partitioning and offloading in heterogeneous cellular networks," *Wireless Communications, IEEE Transactions on*, vol. 13, no. 2, pp. 888–901, February 2014.

[9] H. Tang, J. Peng, P. Hong, and K. Xue, "Offloading performance of range expansion in picocell networks: A stochastic geometry analysis," *Wireless Communications Letters, IEEE*, vol. 2, no. 5, pp. 511–514, 2013.

[10] Q. Ye, B. Rong, Y. Chen, M. Al-Shalash, C. Caramanis, and J. G. Andrews, "User association for load balancing in heterogeneous cellular networks," *Wireless Communications, IEEE Transactions on*, vol. 12, no. 6, pp. 2706–2716, 2013.

[11] B. Soret, H. Wang, K. Pedersen, and C. Rosa, "Multicell cooperation for LTE-Advanced heterogeneous network scenarios," *Wireless Communications, IEEE*, vol. 20, no. 1, pp. 27–34, February 2013.

[12] A. Merwaday, S. Mukherjee, and I. Guvenc, "HetNet capacity with reduced power subframes," in *Wireless Communications and Networking Conference (WCNC), 2014 IEEE*, April 2014, pp. 1380–1385.

[13] T. Novlan, R. Ganti, A. Ghosh, and J. Andrews, "Analytical evaluation of fractional frequency reuse for heterogeneous cellular networks," *Communications, IEEE Transactions on*, vol. 60, no. 7, pp. 2029–2039, July 2012.

[14] M. Cierny, H. Wang, R. Wichman, Z. Ding, and C. Wijting, "On number of almost blank subframes in heterogeneous cellular networks," *Wireless Communications, IEEE Transactions on*, vol. 12, no. 10, pp. 5061–5073, October 2013.

[15] F. Baccelli and B. Blaszczyszyn, *Stochastic Geometry and Wireless Networks, Volume I -Theory*. Hanover, MA, USA: NOW Publisher, 2009.

[16] H. S. Dhillon, R. K. Ganti, F. Baccelli, and J. G. Andrews, "Modeling and analysis of K-tier downlink heterogeneous cellular networks," *Selected Areas in Communications, IEEE Journal on*, vol. 30, no. 3, pp. 550–560, 2012.

[17] W. M. 9. Symbolic integral computation. [Online]. Available: http://www.wolfram.com/mathematica

[18] N. M. Temme, "Large parameter cases of the Gauss hypergeometric function," *Journal of Computational and Applied Mathematics*, vol. 153, no. 12, pp. 441 – 462, 2003, proceedings of the 6th International Symposium on Orthogonal Poly nomials, Special Functions and their Applications, Rome, Italy, 18-22 June 2001.

[19] S. M. Yu and S.-L. Kim, "Downlink capacity and base station density in cellular networks," in *Modeling & Optimization in Mobile, Ad Hoc & Wireless Networks (WiOpt), 2013 11th International Symposium on*. IEEE, 2013, pp. 119–124.